TECHNICAL REPORT ARBRL-TR-02541

NEW SLIDING SURFACE TECHNIQUES ENABLE THE SIMULATION OF TARGET PLUGGING FAILURE

Barbara E. Ringers

December 1983

US ARMY ARMAMENT RESEARCH AND DEVELOPMENT CENTER
BALLISTIC RESEARCH LABORATORY
ABERDEEN PROVING GROUND, MARYLAND

Destroy this report when it is no longer needed.
Do not return it to the originator.

Additional copies of this report may be obtained from the National Technical Information Service, U. S. Department of Commerce, Springfield, Virginia 22161.

The findings in this report are not to be construed as an official Department of the Army position, unless so designated by other authorized documents.

The use of trade names or manufacturers' names in this report does not constitute indorsement of any commercial product.

UNCLASSIFIED

SECURITY CLASSIFICATION OF THIS PAGE *(When Data Entered)*

REPORT DOCUMENTATION PAGE		READ INSTRUCTIONS BEFORE COMPLETING FORM
1. REPORT NUMBER TECHNICAL REPORT ARBRL-TR-02541	2. GOVT ACCESSION NO.	3. RECIPIENT'S CATALOG NUMBER
4. TITLE *(and Subtitle)* NEW SLIDING SURFACE TECHNIQUES ENABLE THE SIMULATION OF TARGET PLUGGING FAILURE		5. TYPE OF REPORT & PERIOD COVERED FINAL 6. PERFORMING ORG. REPORT NUMBER
7. AUTHOR(s) BARBARA E. RINGERS		8. CONTRACT OR GRANT NUMBER(s)
9. PERFORMING ORGANIZATION NAME AND ADDRESS US Army Ballistic Research Laboratory, ARDC ATTN: DRSMC-BLT(A) Aberdeen Proving Ground, MD 21005		10. PROGRAM ELEMENT, PROJECT, TASK AREA & WORK UNIT NUMBERS 1L162618AH80
11. CONTROLLING OFFICE NAME AND ADDRESS US Army AMCCOM, ARDC Ballistic Research Laboratory, ATTN: DRSMC-BLA-S(A) Aberdeen Proving Ground, MD 21005		12. REPORT DATE December 1983 13. NUMBER OF PAGES 41
14. MONITORING AGENCY NAME & ADDRESS*(if different from Controlling Office)*		15. SECURITY CLASS. *(of this report)* UNCLASSIFIED 15a. DECLASSIFICATION/DOWNGRADING SCHEDULE

16. DISTRIBUTION STATEMENT *(of this Report)*

Approved for public release; distribution unlimited.

17. DISTRIBUTION STATEMENT *(of the abstract entered in Block 20, if different from Report)*

18. SUPPLEMENTARY NOTES

19. KEY WORDS *(Continue on reverse side if necessary and identify by block number)*

Terminal Ballistics
Simulation
EPIC-2
Lagrangian
Slide lines
Plugging
Kinetic Energy Penetrator

20. ABSTRACT *(Continue on reverse side if necessary and identify by block number)*

Techniques were developed and incorporated into EPIC-2, a Lagrangian finite element impact code, to accomplish the dynamic relocation of sliding surfaces. This development was necessary in order to model ballistic impact situations involving deep penetration and/or perforation of targets. These techniques were first applied to the modeling of axisymmetric ballistic impact situations involving kinetic energy penetrators versus targets which failed by plugging due to high strains. The development of the criteria required for target failure to begin and proceed "naturally" is included.

DD FORM 1 JAN 73 1473 EDITION OF 1 NOV 65 IS OBSOLETE

UNCLASSIFIED

SECURITY CLASSIFICATION OF THIS PAGE *(When Data Entered)*

TABLE OF CONTENTS

LIST OF ILLUSTRATIONS

I. INTRODUCTION

A major enhancement to the capabilities of EPIC-2,[1] a Lagrangian finite element impact code, has been developed and implemented enabling the modeling of deep penetration and/or perforation of targets. This paper presents the techniques which were developed to handle dynamic relocation of sliding surfaces and the automatic addition of new sliding surfaces when necessary.

These techniques were first applied to the modeling of axisymmetric ballistic impact situations involving kinetic energy penetrators versus targets which fail by plugging due to high strains. The criteria which were required for target failure to begin and proceed "naturally," ultimately resulting in perforation when warranted, are discussed. A parametric study is presented of a hardened, roller bearing steel cylinder impacting a pure titanium target at normal obliquity. Experimentally target failure was considered to be the result of plugging due to high strains. Only the striking velocity and the critical level of equivalent strain necessary to mandate failure were varied in the simulations. The results are demonstrated to be consistent between calculations; furthermore, no rezoning or manual intervention was involved in any of the calculations.

Some discussion is included of a second impact situation similar to the first except that the target was a titanium alloy, Ti 318 (6%Al,4%V). The plugging failure in this situation was considered to be the result of adiabatic shear. It is shown that this case can not be successfully modeled if only the equivalent strain criterion is utilized to predict failure without consideration being given to possible thermal softening in the equations involved.

Also discussed is the extrapolation of these techniques to handle other failure mechanisms, plane strain simulations, and multitarget situations.

II. GEOMETRICAL CONSIDERATIONS

The impetus for this effort was the desire to model ballistic impact situations where the primary mode of target failure was plugging, whether due to high strains or adiabatic shear. In papers by Moss[2] and Zener and Hollomon[3] describing the results of punching experiments, the thicknesses of the shear bands measured

---

[1] *Johnson, G. R., "EPIC-2, A Computer Program For Elastic-Plastic Impact Computations in 2 Dimensions Plus Spin," US Army BRL Contract Report ARBRL-CR-00373, June 1978 (AD A058786).*

[2] *Moss, G. L., "Shear Strains, Strain Rates and Temperature Changes in Adiabatic Shear Bands," US Army BRL Report ARBRL-TR-02242, May 1980 (AD A087765).*

[3] *Zener, C., Hollomon, J. H., "Effect of Strain Rate Upon Plastic Flow of Steel," J. Appl. Phys., V. 15, 1944, 22.*

were in hundredths of a millimeter; the velocities involved were in tens-of-meters/sec. Johnson[4] noted that "the faster a punching operation is, the higher the strain rate and the larger the flow stress but the narrower the shear zone."

In modeling ballistic impacts with EPIC-2, triangular element sizes are typically measured in tenths of a millimeter. Therefore, in simulating a region an order of magnitude smaller, the author decided to let splitting occur between elements when an element has attained a particular failure criterion.

In the original version of EPIC-2, material fracture is simulated by enabling elements which are not master surface elements to fail in two possible ways: 1) failure in shear and tension if the element exceeds specified equivalent or volumetric strain levels, 2) total failure if the element exceeds a specified equivalent strain level. In the first case the element is still able to withstand hydrostatic compression while in the second case all stresses including pressure are set equal to zero.

Since the master sliding surface has to remain intact, only nonmaster elements can be totally failed and therefore only relatively moderate penetration problems can be handled before severe grid deformation in the target essentially halts a calculation.

In the effort discussed in this paper provision was made to totally fail any element, including master surface elements, when it reaches another, as yet unspecified, failure criterion. The rationale was that shearing should be simulated by splitting between elements and that eventually the levels of equivalent strain suffered by some elements would probably require total failure of those elements, simulating erosion.

EPIC-2 initially had two-triangle element arrangements and the choice of orientation of the diagonal between the triangles was left to the user. Johnson[5] recently recommended, however, due to the excessive stiffness of triangular elements in this arrangement, that future EPIC-2 simulations utilize crossed triangles (4 triangles in a quad) arrangement.(Note the element arrangement in Figure 1a.) The geometry generator for this arrangement was therefore utilized in this work.

---

[4] *Johnson, W., Impact Strength of Materials, Edward Arnold Ltd., 1972.*

[5] *Johnson, G. R., "Triangular Element Arrangement for EPIC-2," Internal Memorandum, July 1979.*

III. SLIDING SURFACE TECHNIQUES IN EPIC-2

The original version of EPIC-2 utilizes sliding surfaces comprised of master and slave nodes to keep projectile and target materials separate. For each time increment, the equations of motion are applied to the master nodes (usually the target frontal surface) and the slave nodes (usually those on the projectile surface likely to interact with the target).

The sliding surface routines did not include a double pass, the necessity for which is discussed in Reference 6. Under certain conditions crossovers (interference) occurred between projectile and target materials. Sliding surface routines developed by Lambert[7] which included a double pass for interference--slave nodes versus master surfaces, then master nodes versus slave surfaces--were therefore utilized. If there is interference in the first case the slave node is placed on the master surface in a direction normal to the master surface. Similarly, an interfering master node is placed on the slave surface. Ensuring that translational and rotational momenta are conserved, the velocities of the interfering node and the two nodes comprising the surface involved are updated.

IV. NEW SLIDING SURFACE TECHNIQUES

The author's work involved: 1) enabling splitting between elements 2) enabling the total failure of any element and 3) the dynamic relocation of the master/slave surfaces involved in order to accommodate splitting or element failure. This was necessary in order to handle the modeling of deep penetration and perforation of targets. It is assumed that the slave surface resides on the projectile exterior and the original master surface specified by the user is the frontal target surface. (This is arbitrary and could readily be reversed.)

When an element attains Criterion 1,* indicating that fracture simulated by splitting between elements is to occur, a node is essentially split in two (Figures 1a, 1b); the "split" node retains the original node number, the "new" node is assigned the next node number available. The "split" node, that meeting Criterion 2,* also must be a master node or the element involved is rejected as causing splitting. The direction of the split, determined by a third criterion,* establishes the "next" node, the node from which further splitting must occur.

---

[6] *Johnson, G. R., "Dynamic Analysis of Explosive-Metal Interaction in Three Dimensions," J. Appl. Mech., V. 103, No. 1, March 1981.*

[7] *Lambert, J. P., private communication. Work done at BRL, 1980.*

* *These criteria are defined and discussed in Section VI.*

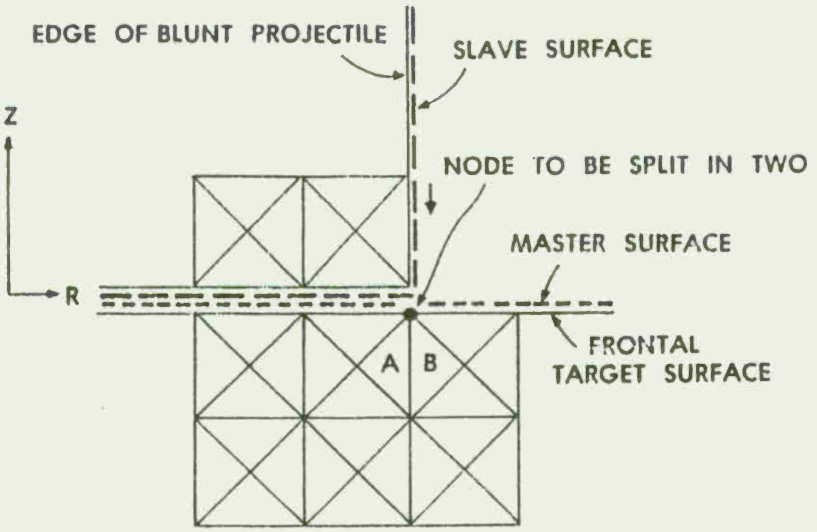

Figure 1a. Element A or B Meets Criterion 1

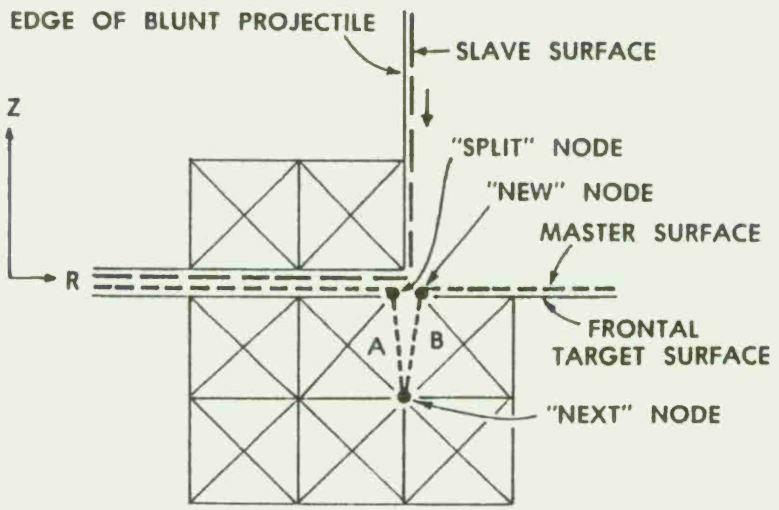

Figure 1b. "Split" Node Meets Criterion 2
Split will be Furthered from Next Node

Once the "split," "new," and "next" nodes are determined, the elements are assigned the "split" or "new" node depending on which side of the split they reside. Both the "next" node and the "new" node are now inserted in the master surface after the original "split" node, thereby dynamically relocating this sliding surface.(See Figure 2a.) The "new" node is assigned the same coordinates, velocities and restraint properties as the "split" node. The masses assigned to the "split" and "new" nodes are based on which elements now share each node. The forces assigned the "split" and "new" nodes are based on the ratios of the newly assigned nodal masses to the original pre-split nodal mass.

Besides interference between the projectile (slave surface) and target (master surface), there must be concern about possible interference between the two sides of the split developing in the target. This is handled by establishing another set of master/slave surfaces whose mutual interference is checked identically to the first set. The second slave surface is considered to be the first master surface up to and including the original "split" node. The second master surface is considered to be the first master surface starting with the "next" node, the second node being the "new" node.(See Figure 2b.) This was also done arbitrarily in that the second master and slave surfaces could reverse positions and the result should be the same.

Interference between master and slave surfaces is based on the stipulation that the slave surface remains to the left of the master surface proceeding in the increasing direction of the sliding surface. A necessary addition to the sliding surface treatment was the consideration of an interposing surface between a supposed interfering slave or master node and a corresponding master or slave surface.(See Figure 3.) The master node M is to the right of slave surface S1 but it is also to the left of slave surface S2. M therefore appears to be interfering with S2 but surface S1 interposes so M does not validly interfere.

The split continues until either the projectile velocity reaches zero or until target perforation occurs. When the "next" node is positioned on the distal target surface, perforation is imminent; a discontinuity in the sliding surface enables complete separation of the plug from the remaining target material. There is no further test for elements reaching Criterion 1.

V. EXPERIMENTAL IMPACT SITUATIONS

Two experimental impact situations served as a basis for this study and were conducted and discussed by Woodward.[8] Both impact situations involved a blunt, hardened, roller bearing steel cylinder impacting titanium targets at 0^{o} obliquity. In the

---

[8] *Woodward, R. L., "The Penetration of Metal Targets Which Fail By Adiabatic Shear Plugging," Int. J. Mech. Sci., V. 20, 1978, 599-607.*

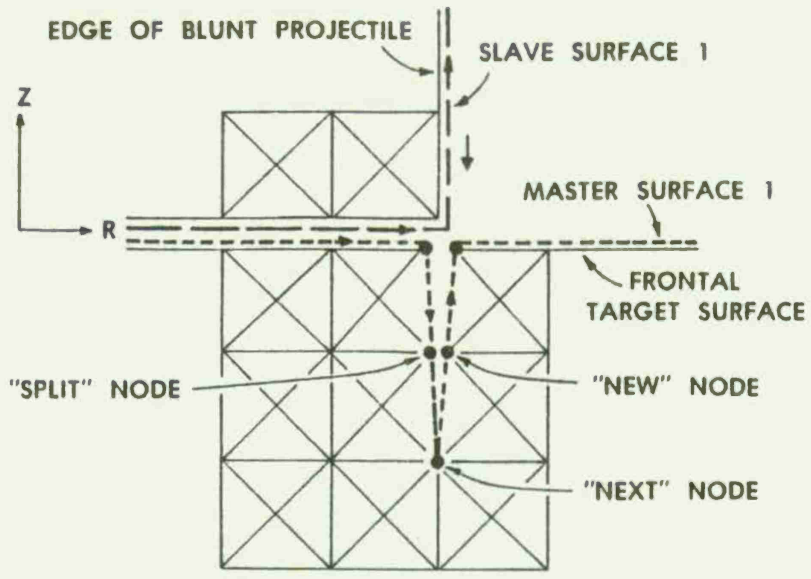

Figure 2a. Sliding Surface 1 Interactions

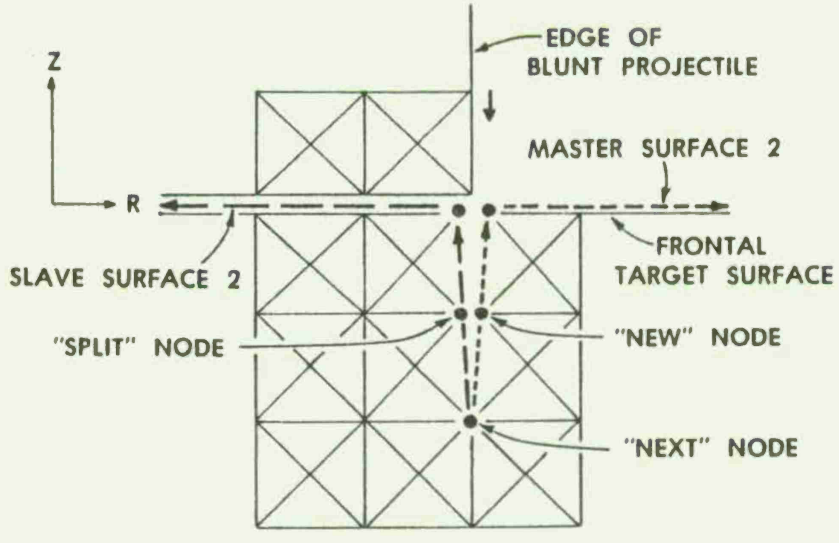

Figure 2b. Sliding Surface 2 Interactions

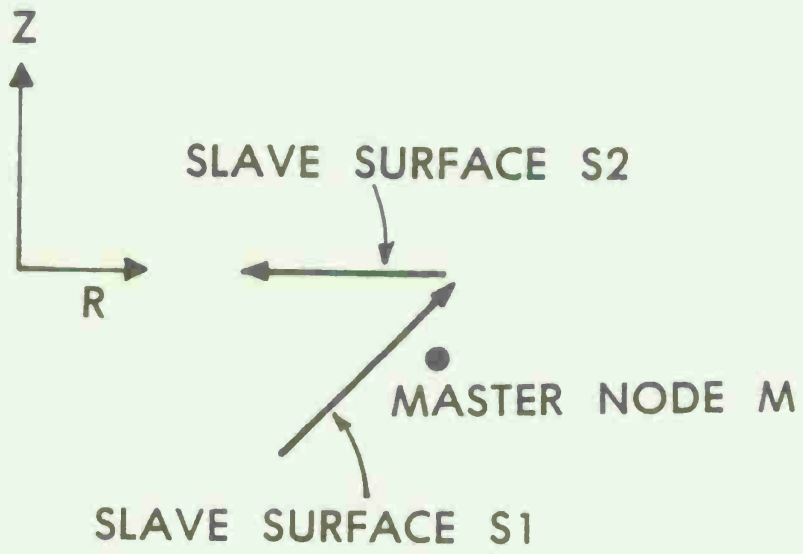

Figure 3. Interposing Surface

first case the titanium target was 99% pure titanium (Ti 125) and target failure was considered to be the result of plugging due to high strains.(See Table 1 for specifics on impact situation.) In the second case the target was a titanium alloy, Ti 318 (6%Al,4%V), and target failure was the result of plugging due to adiabatic shear.

The first case is the basis for the parametric study presented. The expected energy to accomplish perforation of the Ti 125 target with a blunt cylinder was estimated to be 148 joules (Reference 8) implying a critical velocity of approximately 300 m/s.

Prior to enabling splitting between elements, the simulation was attempted with a striking velocity of 350 m/s to assure perforation; this was run for 10 μs, the deformation pattern of which is shown in Figure 4a, indicating the formation of an incipient shear band. The deformed target elements around the projectile periphery suffered an equivalent strain of 300% by 10 μs.

Contrast these results with those for the simulation of the second case, the target material being Ti 318 (Figure 4b). There is no sign of a shear band by 10 μs. The highest strain suffered by an element in the top layer was 88%, the highest second layer element having reached only 13% strain. Clearly, adiabatic shear can not be successfully modeled without the addition of mathematical formulation to include thermal softening. Ti 125 has a far lower strength and a higher strain hardening rate than Ti 318. This would seem to be in agreement with Recht's criterion[9] that a high shear yield stress and low strain hardening rate are conducive to adiabatic shear.

VI. DEVELOPMENT OF CRITERIA MANDATING TARGET FAILURE

After the mechanical techniques described in Section IV were implemented, the author developed criteria which had to be met for the initiation and furthering of the splitting between elements to occur. A criterion which remained constant during this study was the initiation and continuation of a split past an element having attained a critical level of equivalent strain $\bar{\varepsilon}$ (Criterion 1).

According to Crandall, Dahl, and Lardner,[10] describing the yielding tendency in terms of equivalent stress and equivalent plastic strain appears to correlate well with data when the ratios of the principal stresses remain constant during the test

---

[9] *Recht, R. F., "Catastrophic Thermoplastic Shear," J. Appl. Mech. Trans., ASME31E, 1964, 189.*

[10] *Crandall, S. H., Dahl, N. C., and Lardner, T. J., "An Introduction to The Mechanics of Solids," McGraw-Hill, 1978.*

Table 1. Projectile and Target Properties

	PROJECTILE	*TARGET 1 (Ti 125)*	*TARGET 2 (Ti 318)*
MATERIAL	HARDENED, ROLLER BEARING STEEL	ROLLED & ANNEALED 99% PURE Ti	Ti WITH 6% Al, 4% V
SHAPE	BLUNT	50 mm SQUARE	50 mm SQUARE
MASS	3.34 g	—	—
LENGTH	25.4 mm THICK	6.35 mm	6.35 mm
DIAMETER	4.76 mm	—	—
DENSITY	7.39×10^3 kg/m^3	4.51×10^3 kg/m^3	4.43×10^3 kg/m^3
YIELD σ_Y	2290 MPa	522.5 MPa	1029 MPa
UTL σ_U	2500 MPa	600 MPa	1209 MPa
ϵ_U	∞	.45 - .5	.2
SPEC HEAT	4.6×10^2 J/kg °C	5.1916×10^2 J/kg °C	5.65×10^2 J/kg °C
YOUNGS MOD	1.93×10^5 MPa	1.158×10^5 MPa	1.158×10^5 MPa

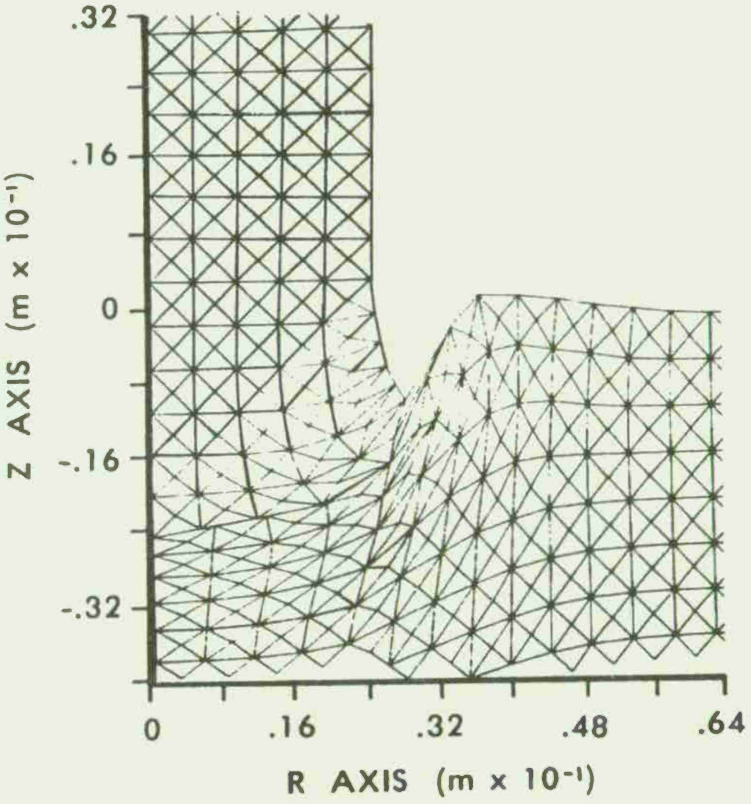

Figure 4a. Steel Cylinder versus Ti 125 Target

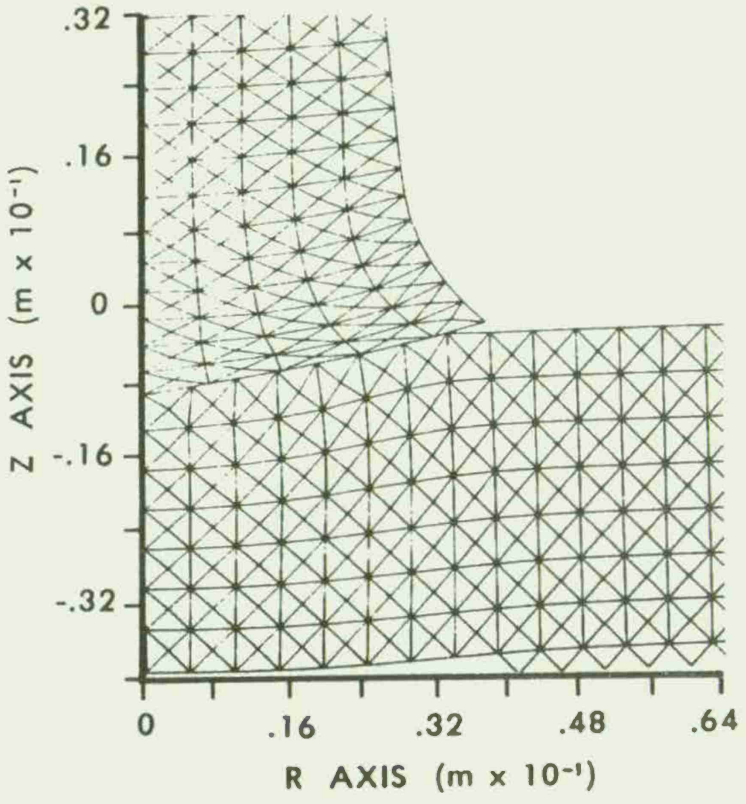

Figure 4b. Steel Cylinder versus Ti 318 Target

and appreciable anisotropy is not developed during straining. "The components of strain derived from the Mises yield criterion are much closer to physical observations than those found from the maximum shear-stress criterion."[10]

Another criterion (Criterion 2) which remained constant was the choice of the initial "split" node. The node suffering the highest force associated with the first element meeting Criterion 1 was selected to be the initial "split" node. It was also required that this node be a master node or the element would be rejected as one enabling split to occur. After splitting was initiated, only those elements associated with the "next" node were considered for possible furthering of the split. Since the primary objective of this effort was to model target failure, and little projectile deformation was expected in the case of the Ti 125 target impact, the projectile elements were not allowed to fail.

The direction of the split (Criterion 3), the critical level of Criterion 1, and amendments to Criterion 1 varied during the solutions attempted. The following is a summary of the principal approaches taken and the results of each:

1) Require only a specific level of $\bar{\varepsilon}$ for an element to cause splitting. Results: a) Surface elements not contiguous to the projectile periphery suffered sufficient compression to attain $\bar{\varepsilon}$ first. b) Splitting would proceed in one direction while the thrust of the problem proceeded in another.

2) Require relatively high levels of $\bar{\varepsilon}$ (ie. 300%) for an element to cause splitting. Results: Calculation took far too long with only slight penetration predicted for an experimental situation in which perforation resulted.

3) Base the direction of the split on nodal forces. Results: Nodal forces fluctuated widely; the split proceeded in one direction while the thrust of the problem proceeded in another.

4) Let the split close up if the thrust of the problem went in a different direction, enabling the split to be furthered from a node other than the "next" node. Results: intractable.

The following criteria which resulted in natural and pleasing results consistent with the thrust of the impact and consistent between problems were utilized in the parametric investigation of the impact situation described in Section V.

Criterion 1: An element initiates or furthers a split
1) when its equivalent strain ($\bar{\varepsilon}$) reaches a user-specified critical level,
2) if, in furthering a split, it is associated with the "next" node,
3) if the magnitude of its shear stress is greater than the magnitude of its axial or radial deviator stress, and
4) if the direction of the split (Criterion 3) does not change by 90° or more.

Criterion 2: The node at which initial splitting occurs
1) must belong to the element meeting Criterion 1,
2) must suffer the highest force of all three nodes belonging to the same element, and
3) must be a master node.

Criterion 3: The direction of the split is determined by the strain of the element meeting Criterion 1. If the magnitude of the axial strain is greater than the magnitude of the radial strain, splitting is to the nearer radial node. Otherwise, splitting is to the nearer axial node.

A discussion of some of the criteria is in order. Obviously, every attempt was made to ensure the workability of an equivalent strain criterion. It does not seem unreasonable to require the line of major fracture to continue from the "next" node and without a major (90°) change in direction. However, the requirement that the magnitude of the shear stress be greater than the magnitudes of the axial and radial deviator stresses may not be satisfying in a continuum mechanics sense. This may, in essence, be invoking a maximum shear stress criterion.

Maximum Shear Stress

$$\tau_{max} = 1/2\sqrt{(\sigma_r - \sigma_z)^2 + 4\tau_{rz}^2} \tag{1}$$

where the radial stress

$$\sigma_r = \bar{\sigma}_r + \frac{\sigma_r + \sigma_z + \sigma_\theta}{3}, \tag{2}$$

the axial stress

$$\sigma_z = \bar{\sigma}_z + \frac{\sigma_r + \sigma_z + \sigma_\theta}{3}, \tag{3}$$

τ_{rz} is the shear stress acting on the axial-radial plane, and $\bar{\sigma}_r$, $\bar{\sigma}_z$ are the radial and axial deviator stresses and the expression $\frac{\sigma_r + \sigma_z + \sigma_\theta}{3}$ is the hydrostatic stress. Therefore,

$$\tau_{max} = 1/2\sqrt{(\bar{\sigma}_r - \bar{\sigma}_z)^2 + 4\tau_{rz}^2} \quad (4)$$

Both the radial and axial deviator stresses have the same sign (-) so this expression reduces the effect of both, making the shear stress the crucial parameter. However, in redoing the first calculation for 30 μs and determining the maximum shear stress, some of the top elements modeling the target surface suffered sufficient compression to make the maximum shear stress calculated very close to that for the first element at the projectile periphery which was allowed to start splitting. Since experimental evidence did not exist with regard to the target erosion involved, the conservative position was taken that elements would only be totally failed when a minimum time increment violation occurred.

VII. RESULTS OF PARAMETRIC STUDY

Four variations on the first ballistic impact situation, a hardened, roller bearing steel cylinder versus a Ti 125 (99% titanium) target, are presented. The projectile and target properties remain the same for each (projectile and target 1 properties in Table 1).

The first calculation was made primarily to test out the techniques developed enabling splitting. A striking velocity of 500 m/s and a critical $\bar{\varepsilon}$ =100% were utilized to ensure a relatively fast calculation and one assuredly resulting in perforation. At 35.6 μs perforation did occur. This was the only calculation in which a minimum time increment violation occurred (at 44.7 μs) in a highly stressed element to the right of the plug. The element was automatically totally failed for a minimum time increment violation and the calculation continued. By 45 μs the projectile was no longer affected by the remaining target material and the residual velocity had settled to 237 m/s. If this were a multiple target situation, this would be the appropriate time to discard the first target (except for the plug) and add a second target. This could be done relatively easily and automatically because the velocities of the plug nodes were an order of magnitude greater than the nodes representing the remaining target material. The deformation plots detailing the progress are shown in Figure 5. The pattern of elements which initiated and furthered splitting and the times at which they did so are shown in Figure 6.

For the second through fourth calculations, a striking velocity of 350 m/s was utilized as it was closer to the experimental situation being modeled. A critical $\bar{\varepsilon}$ of 100% was utilized for the second calculation, as with the first calculation. The projectile penetrated 5.08 mm before rebounding

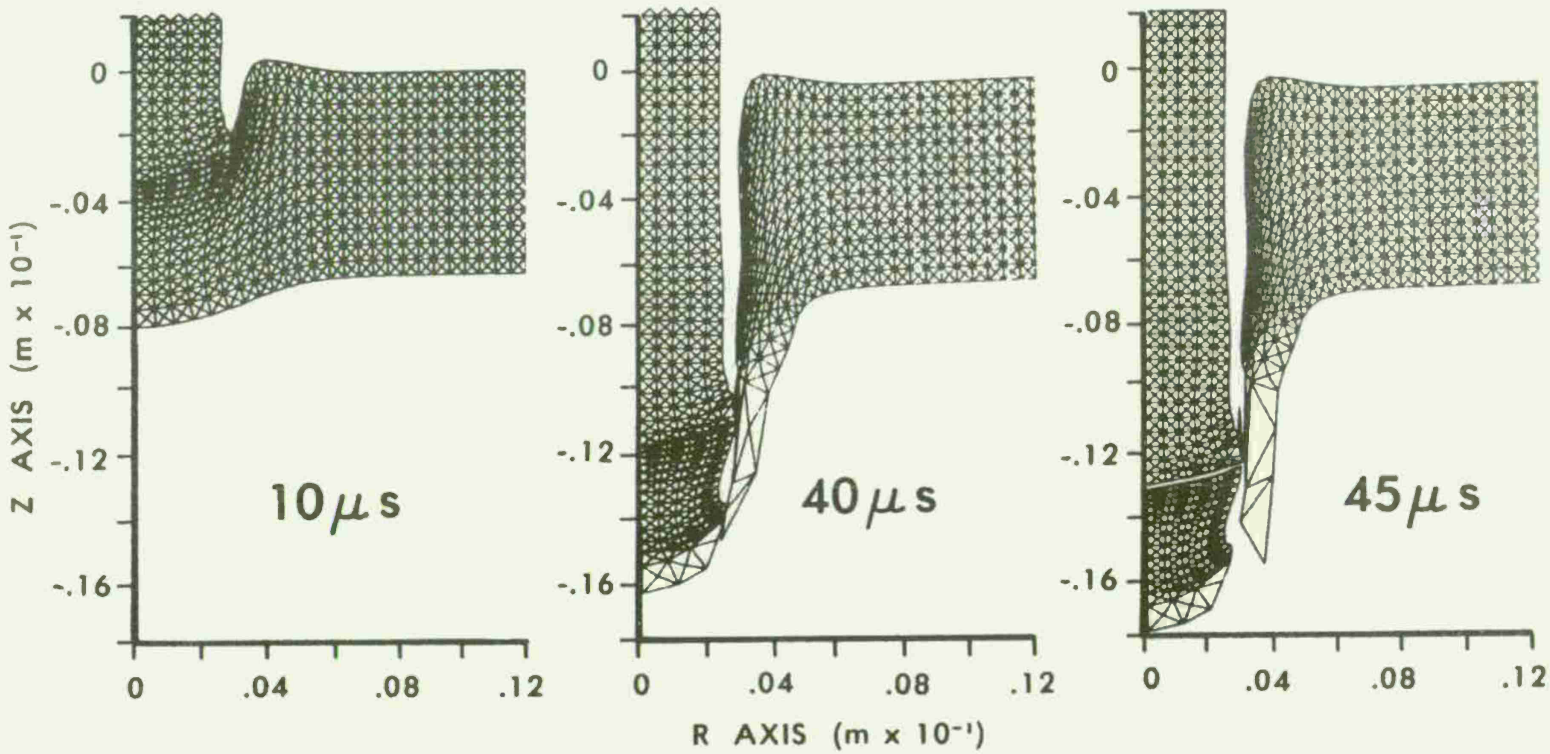

V_S = 500 m/s

$\bar{\epsilon}$ = 1

PERFORATION @ 35.6 μs

V_R = 237 m/s

Figure 5. Deformation History - Calculation 1

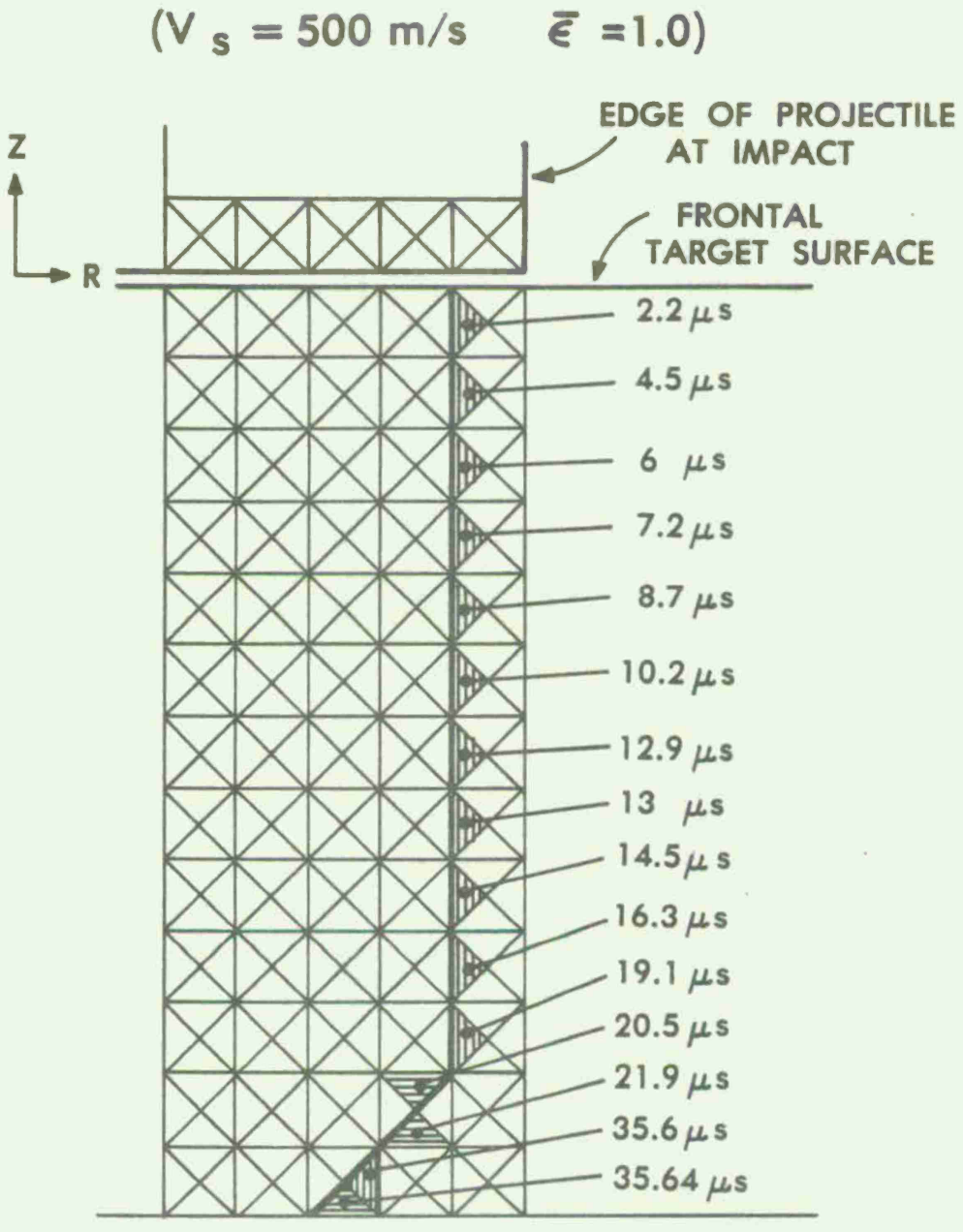

Figure 6. Pattern of Elements Initiating or Furthering Split - Calculation 1

at 40 μs; splitting past six elements and layers had occurred. This calculation was allowed to continue until the rebound velocity stabilized at 27.4 m/s by approximately 70 μs. The deformation plots showing its progress are shown in Figure 7.

The critical $\bar{\varepsilon}$ was reduced to .75 for the third calculation in an effort to obtain perforation at 350 m/s. The projectile penetrated further, to 5.49 mm, before rebounding at approximately 45 μs, reaching a rebound velocity of 20 m/s by 50 μs. In this calculation, splitting had occurred past nine elements (layers) before rebound occurred. The deformation plots showing its progress are shown in Figure 8.

For the fourth calculation, the critical $\bar{\varepsilon}$ was reduced to .5, the rationale for the validity of such a low level being that the ultimate strain for the target material is ε_u =.45-.5. This time perforation did occur, at 28.8 μs. The deformation plots showing its progress through 70 μs are shown in Figure 9. The pattern of elements which initiated and furthered splitting are shown in Figure 10. This is perhaps the most interesting case in that perforation occurred, a plug was completely formed, yet there was not sufficient energy for the penetrator and plug to continue past the remaining target. Instead, the projectile finally rebounded and, at 70 μs, had a rebound velocity of 7 m/s while the plug was still moving in the opposite direction past the remaining target material at 24 m/s. By 90 μs the plug was essentially stuck in the target.

For all four calculations the projectile speed histories are shown in Figure 11; the depth of penetration histories are shown in Figure 12. In all calculations there was no manual intervention or rezoning involved as the problems progressed. Clearly, the results are consistent between calculations, a higher striking velocity producing perforation and a free-flying projectile and plug whereas the lower velocity resulted in projectile rebound. A lower level of critical $\bar{\varepsilon}$ enabled complete formation of a plug and perforation whereas higher levels of critical $\bar{\varepsilon}$ resulted in considerable penetration but no perforation. The time of perforation in both calculations 1 and 4 indicates average crack velocities of 178 m/s and 220 m/s, respectively.

The deformation plots indicate large volumetric strains for the distal target elements by 40 μs, particularly for the first case. Woodward[11] suggested that it might be due to a buildup of hydrostatic tension. The hydrostatic tension had been limited to one third of the ultimate strength of the material in the calculation. The calculation was rerun with the hydrostatic tension limited to 100% of the ultimate strength; the "blowup" of the distal target elements disappeared. (See Figure 13.)

---

[11] *Woodward, R. L., private communication.*

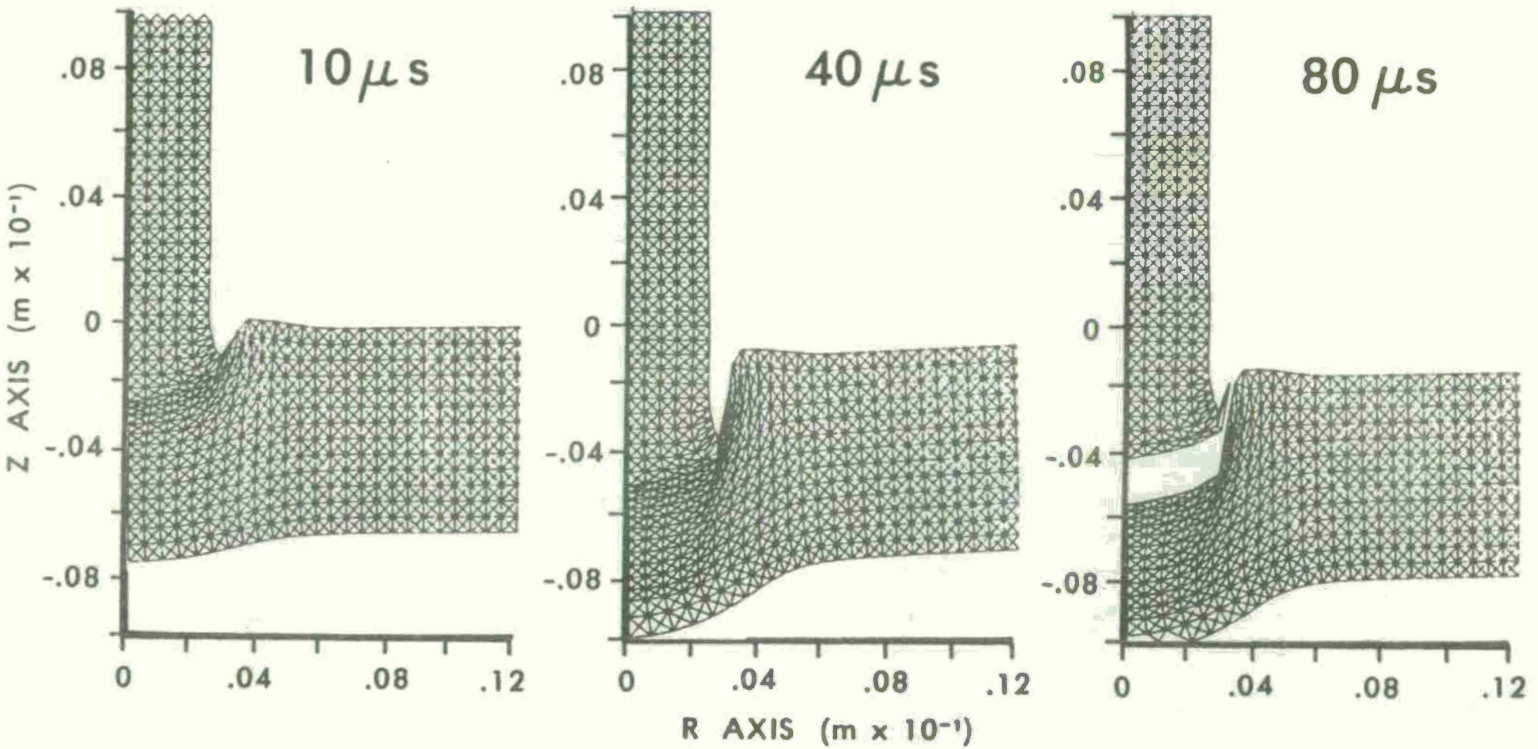

V_S = 350 m/s

$\bar{\epsilon}$ = 1

SPLIT THROUGH 6 LAYERS

REBOUND @ 40 μs

V_{REB} = 27.4 m/s

DEPTH OF PENETRATION = 5.08 mm

Figure 7. Deformation History - Calculation 2

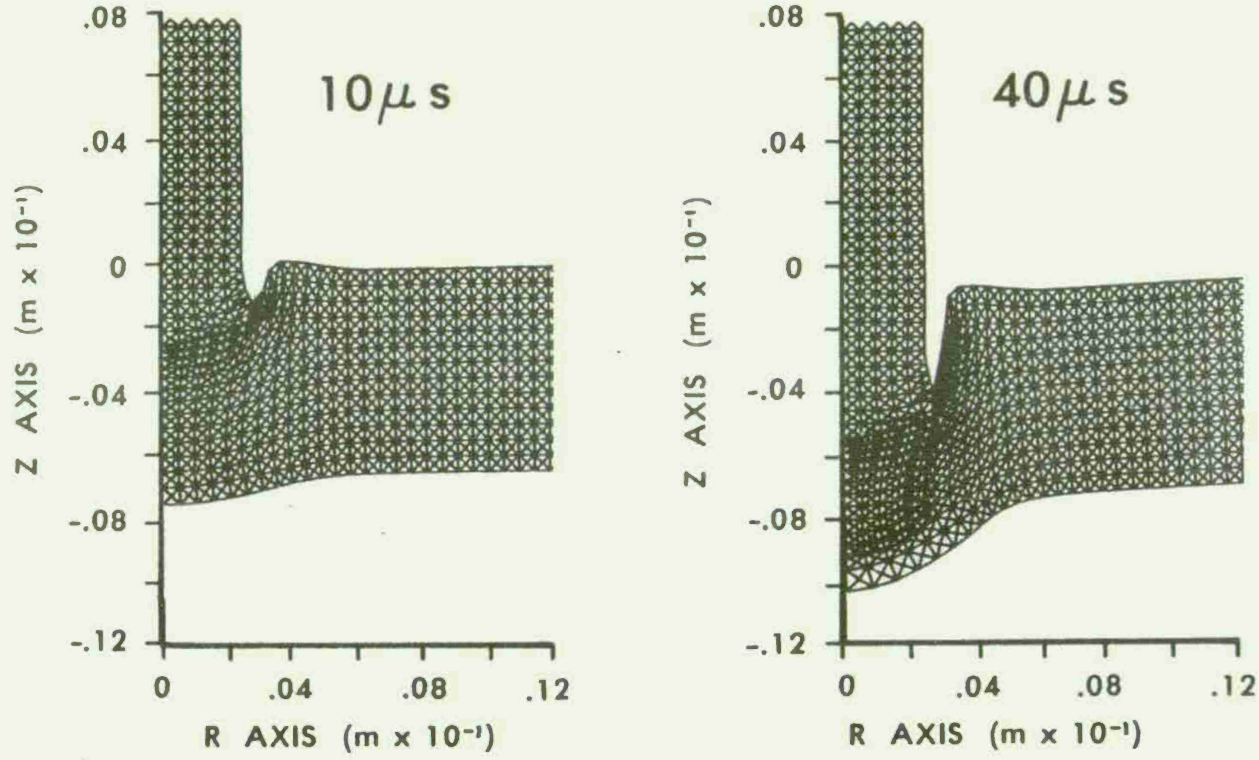

V_S = 350 m/s

$\bar{\epsilon}$ = .75

SPLIT THROUGH 9 LAYERS

REBOUND @ 45μs

V_{REB} 20 m/s @ 50μs

DEPTH OF PENETRATION = 5.49 mm

Figure 8. Deformation History - Calculation 3

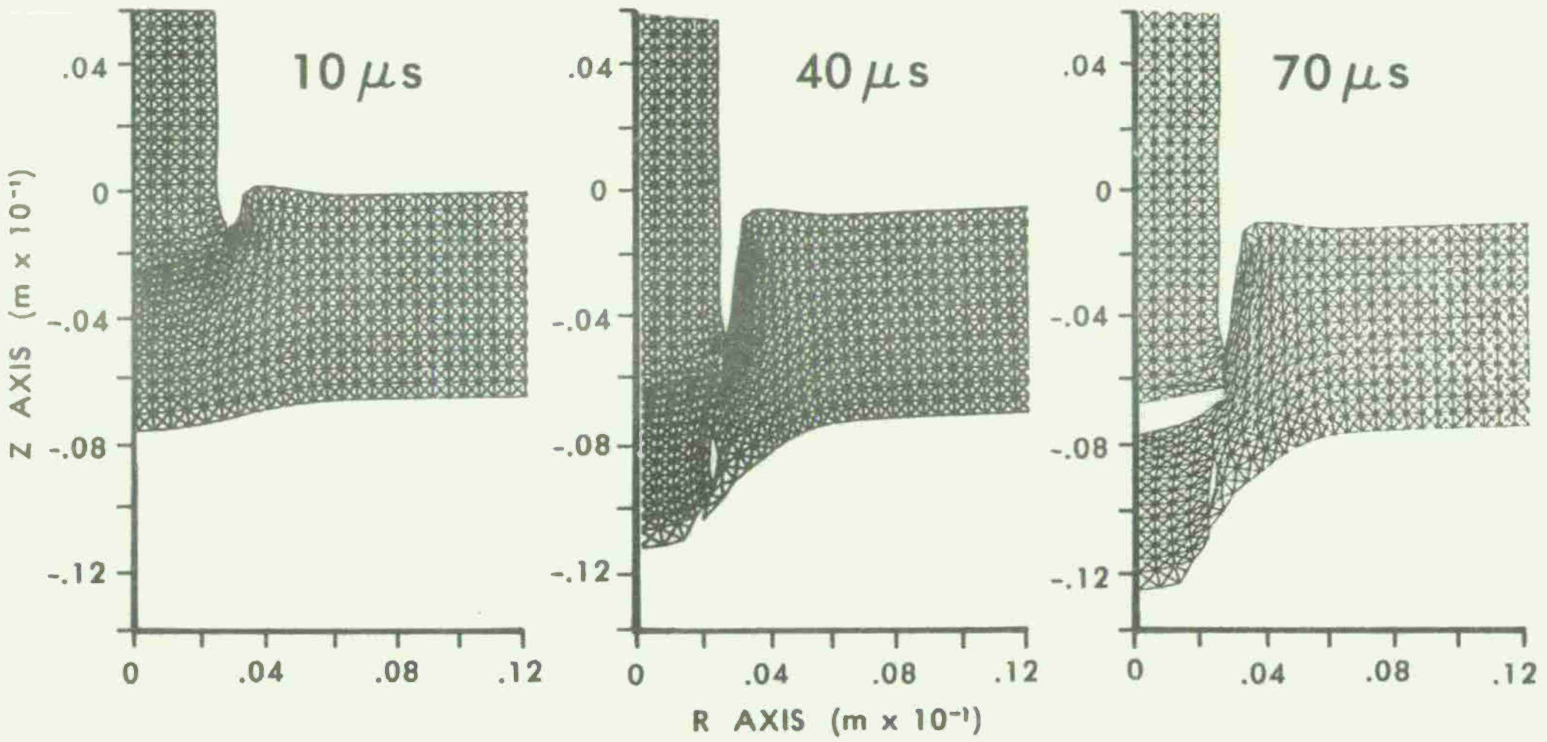

V_S = 350 m/s

$\bar{\epsilon}$ = .5

PERFORATION AT 28.8 μs

REBOUND @ 60 μs

V_{REB} = 7 m/s @ 70 μs

V_{PLUG} = 24 m/s

Figure 9. Deformation History - Calculation 4

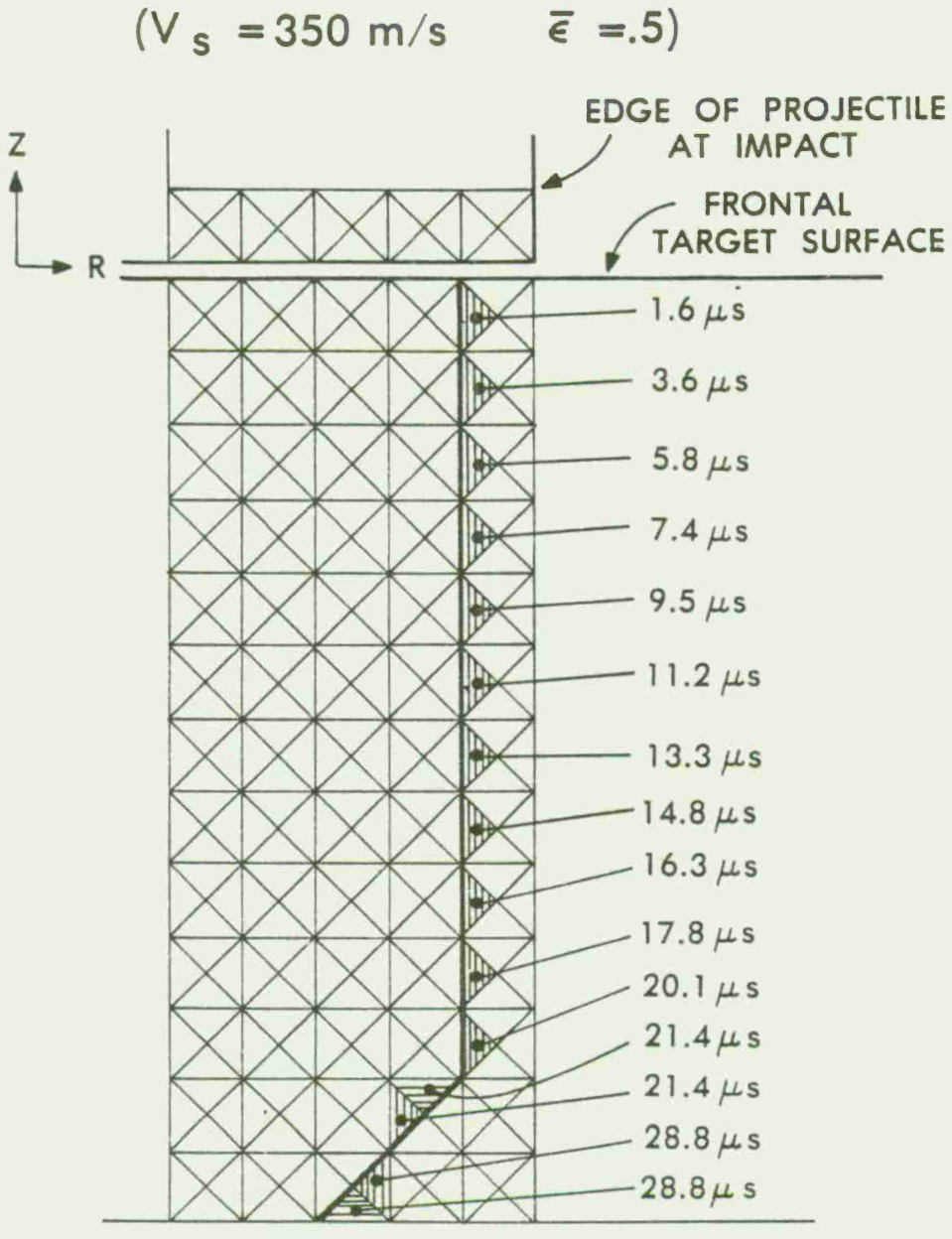

Figure 10. Pattern of Elements Initiating or Furthering Split - Calculation 4

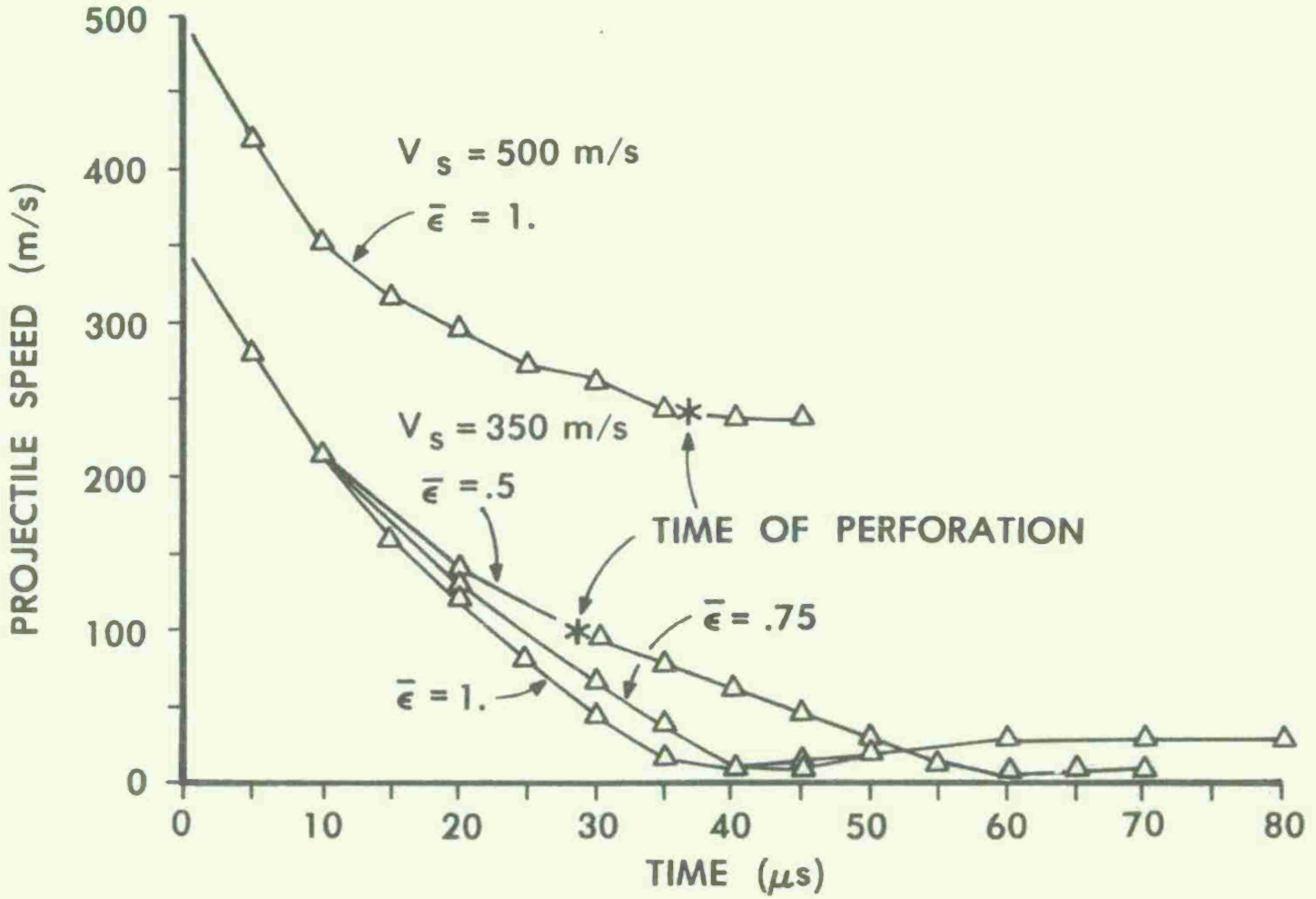

Figure 11. Projectile Speed Histories - Calculations 1 - 4

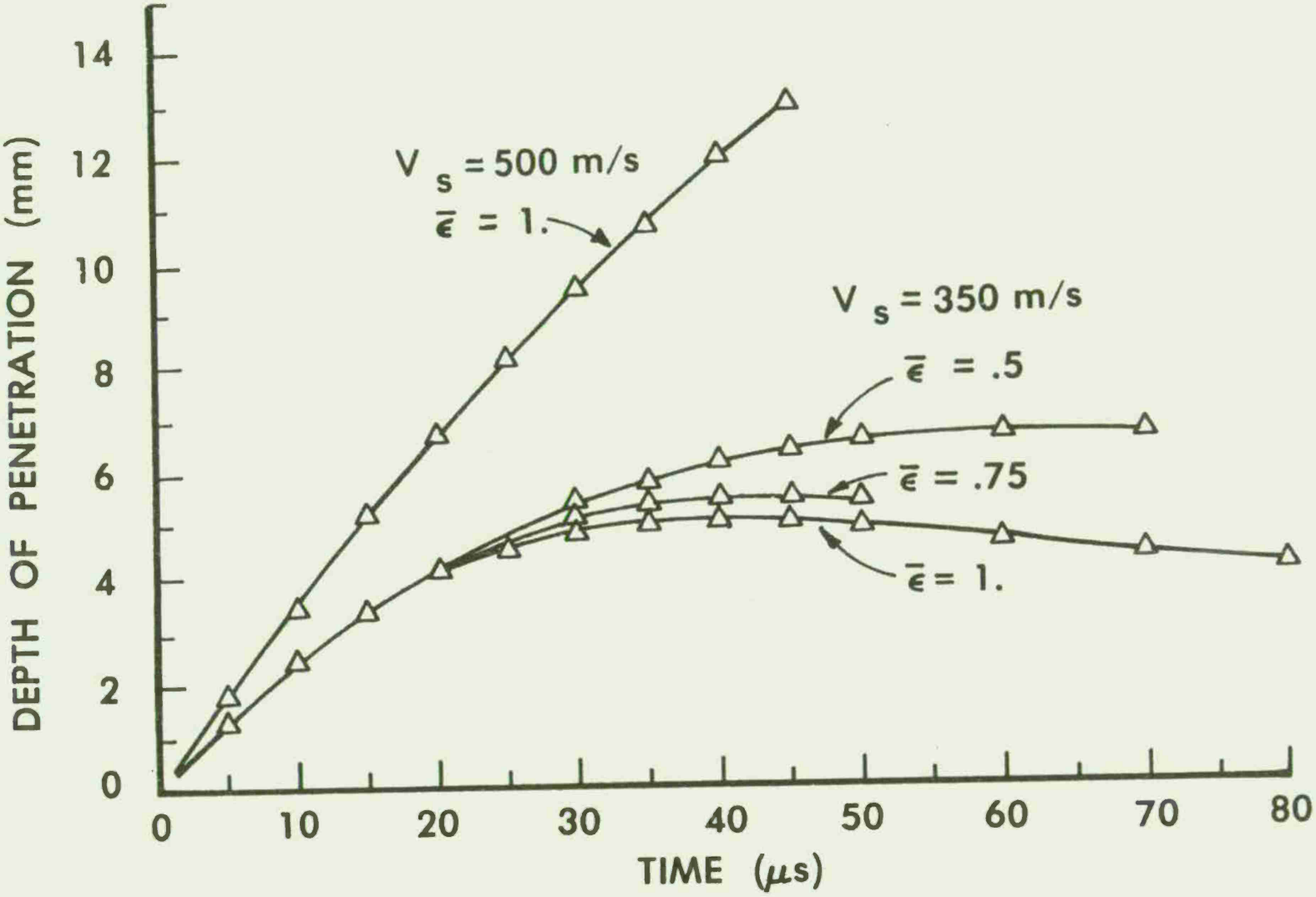

Figure 12. Projectile Depth-of-Penetration History - Calculations 1 - 4

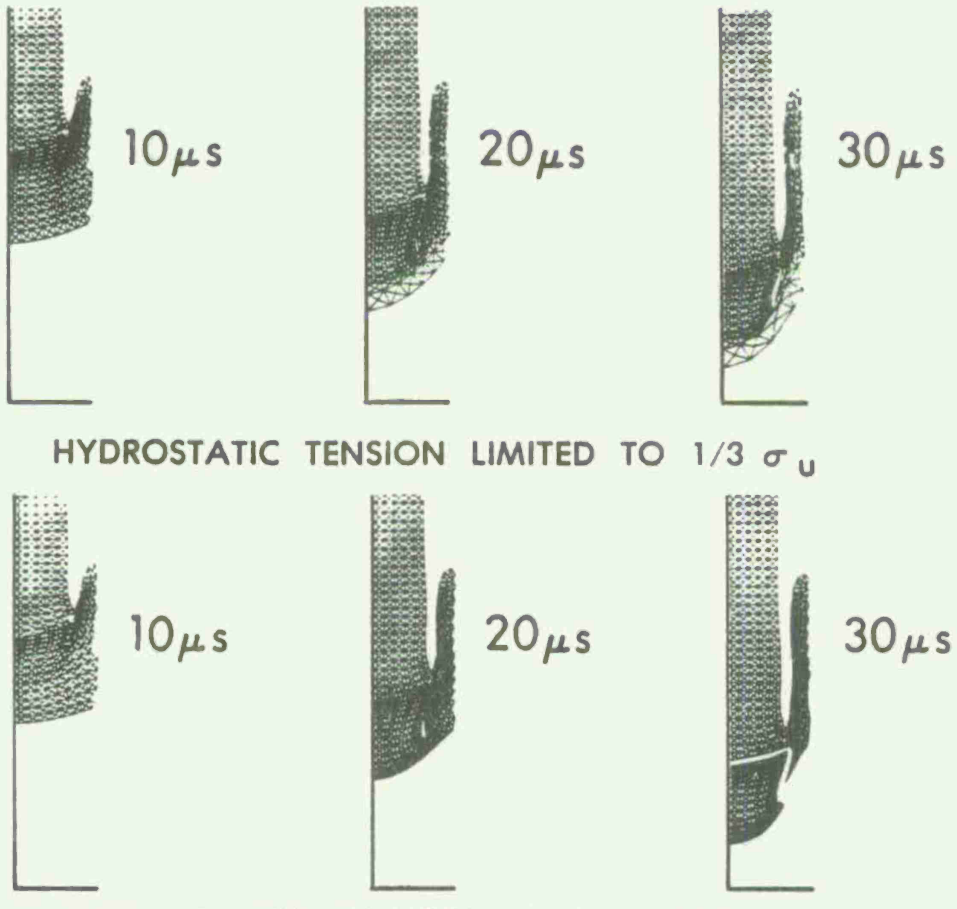

Figure 13. Comparison of Results with Different Hydrostatic Tension Limitations

Whereas the compressive wave traveled unhindered through to the rear of the target, the tensile wave was reflected from the rear of the target and limited to one third of the ultimate strength of the material. Therefore, the rear surface elements received the brunt of the tensile wave, passing on only a severely reduced tensile wave to the interior elements. In the second case, there was no such limitation on the tensile wave, thereby spreading the effect more evenly.

VIII. EXTRAPOLATION OF TECHNIQUES TO OTHER IMPACT SITUATIONS

A. Axisymmetric, Piercing Failure Simulations

For axisymmetric simulations of piercing failure, the techniques discussed in Section IV can be utilized with regard to the generation of the "split" and "next" nodes. However, symmetry is about the z axis and the nodes along the z axis are restrained radially. If the "next" node is restrained at the z axis (Figure 14) then it simply becomes the first node on the master sliding surface and the "split" node is not split; instead, it is released from its restraint at the z axis. Until an unrestrained node becomes the "next" node, there is no generation of new master and slave surfaces.

B. Plane Strain Simulations

The techniques discussed in Section IV can also be utilized in plane strain simulations, the primary difference being the need to generate a third, as well as a second, sliding surface to handle plugging failure. The development of the third sliding surface would proceed exactly as the second. The subsequent inefficient and unnecessary overlap of second master surface with the third slave and master surfaces could be eliminated by choosing a convenient midpoint at which to arbitrarily end the second master surface and begin the third slave surface. (See Figure 15.)

C. Multitarget Situation

Once target nodes and elements other than those comprising a plug are no longer affected by the projectile, modifications can be instituted to eliminate those target nodes with sufficiently low velocity and their associated elements. In the calculation presented, the plug nodes had velocities which were an order of magnitude greater than the remaining target nodes. The second (and third, if for a plane strain simulation) sliding surface can then be eliminated and a second target surface generated. The various, possibly complex, sliding surface interactions which would be necessary would depend on the particular new target situation and whether the projectile and plug stayed together while impacting the second target.

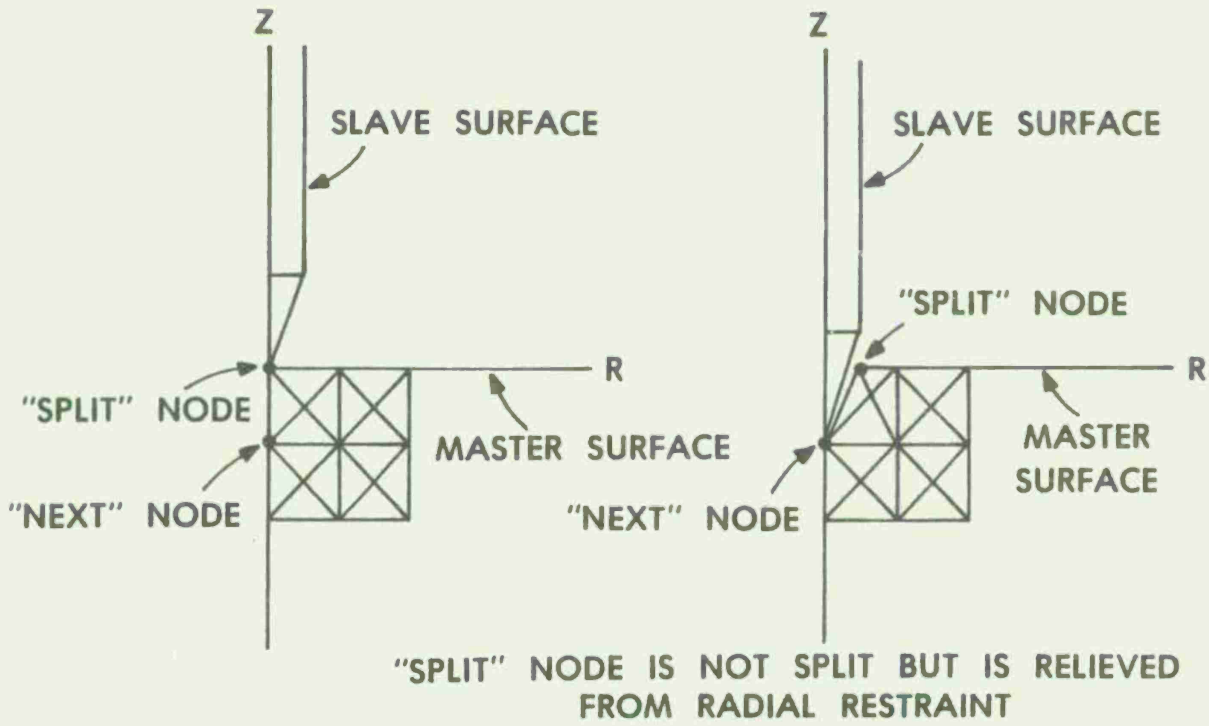

Figure 14. Axisymmetric Piercing Failure Simulations

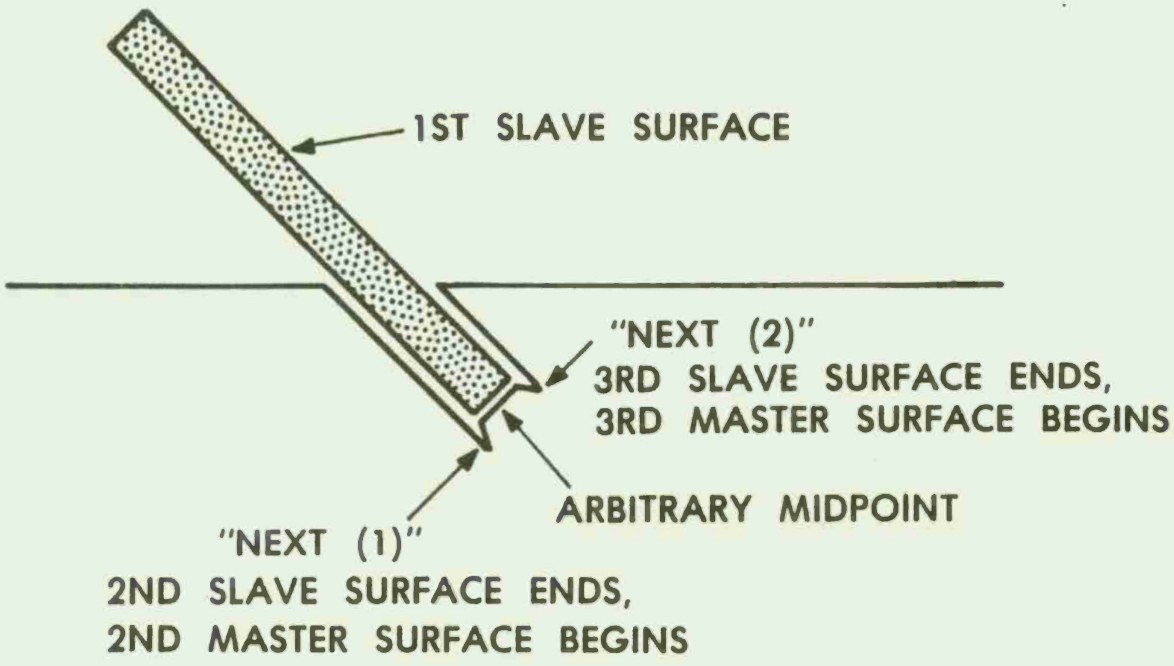

Figure 15. Plane Strain Simulations

IX. CONCLUSIONS

Techniques have been described which enable the dynamic relocation of sliding surfaces and addition of new ones, when necessary, in order to enable EPIC-2 to handle deep penetration/perforation of targets in ballistic impact simulations. These techniques were first applied to an axisymmetric ballistic impact test case where plugging was the primary failure mode. The development of criteria which determined the occurrence of fracture "naturally" as well as a parametric study of a normal impact situation involving plugging failure were presented. Future work includes utilizing these techniques in attempting to model plugging due to adiabatic shear, the extrapolation of these techniques to model other target failure situations such as piercing, plane strain simulations, and the marriage of splitting and erosion techniques. It should now be feasible to consider utilizing this modified Lagrangian code to address multiple target situations as well.

REFERENCES

1. Johnson, G. R., "EPIC-2, A Computer Program For Elastic-Plastic Impact Computations in 2 Dimensions Plus Spin," US Army BRL Contract Report ARBRL-CR-00373, June 1978 (AD A058786).

2. Moss, G. L., "Shear Strains, Strain Rates and Temperature Changes in Adiabatic Shear Bands," US Army BRL Report ARBRL-TR-02242, May 1980 (AD A087765).

3. Zener C., Hollomon, J. H., "Effect of Strain Rate Upon Plastic Flow of Steel," J. Appl. Phys., V. 15, 1944, 22.

4. Johnson, W., Impact Strength of Materials, Edward Arnold Ltd., 1972.

5. Johnson, G. R., "Triangular Element Arrangement For EPIC-2," Internal Memorandum, July 1979.

6. Johnson, G. R., "Dynamic Analysis of Explosive-Metal Interaction in Three Dimensions," J. Appl. Mech., V. 103, No. 1, March 1981.

7. Lambert, J. P., private communication. Work done at BRL, 1980.

8. Woodward, R. L., "The Penetration of Metal Targets Which Fail By Adiabatic Shear Plugging," Int. J. Mech. Sci., V. 20, 1978, 599-607.

9. Recht, R. F., "Catastrophic Thermoplastic Shear," J. Appl. Mech. Trans., ASME31E, 1964, 189.

10. Crandall, S. H., Dahl, N. C., and Lardner, T. J., "An Introduction to The Mechanics of Solids," McGraw-Hill, 1978.

11. Woodward, R. L., private communication.

DISTRIBUTION LIST

No. of Copies	Organization
12	Administrator Defense Technical Info Center ATTN: DTIC-DDA Cameron Station Alexandria, VA 22314
1	Commander US Army Materiel Development and Readiness Command ATTN: DRCDMD-ST 5001 Eisenhower Avenue Alexandria, VA 22333
1	Commander Armament R&D Center US Army AMCCOM ATTN: DRSMC-TDC(D) Dover, NJ 07801
2	Commander Armament R&D Center US Army AMCCOM ATTN: DRSMC-TSS(D) Dover, NJ 07801
1	Commander US Army Armament, Munitions and Chemical Command ATTN: DRSMC-LEP-L(R) Rock Island, IL 61299
1	Director Benet Weapons Laboratory Armament R&D Center US Army AMCCOM ATTN: DRSMC-LCB-TL(D) Watervliet, NY 12189
1	Commander US Army Aviation Research and Development Command ATTN: DRDAV-E 4300 Goodfellow Blvd St. Louis, MO 63120
1	Commander US Army Communications Rsch and Development Command ATTN: DRSEL-ATDD Fort Monmouth, NJ 07703
1	Commander US Army Electronics Research and Development Command Technical Support Activity ATTN: DELSD-L Fort Monmouth, NJ 07703
1	Commander US Army Missile Command ATTN: DRSMI-R Redstone Arsenal, AL 35898
1	Commander US Army Missile Command ATTN: DRSMI-YDL Redstone Arsenal, AL 35898
1	Commander USA Tank Automotive Command ATTN: DRSTA-TSL Warren, MI 48090
1	Director US Army TRADOC Systems Analysis Activity ATTN: ATAA-SL WSMR, NM 88002
2	Commandant US Army Infantry School ATTN: ATSH-CD-CSO-OR Fort Benning, GA 31905
1	AFWL/SUL Kirtland AFB, NM 87117
1	Director US Army Air Mobility Research and Development Laboratory Ames Research Center Moffett Field, CA 94035

DISTRIBUTION LIST

No. of Copies	Organization
2	Commander Naval Air Development Center, Johnsville Warminster, PA 18974
1	Commander Naval Missile Center Point Mugu, CA 93041
2	Commander Naval Ship Engineering Center ATTN: J. Schell Tech Lib Washington, DC 20362
1	Commander David W. Taylor Naval Ship Research & Development Center ATTN: Code 1740.4, R. A. Gramm Bethesda, MD 20084
3	Commander Naval Surface Weapons Center ATTN: Dr. W. G. Soper Mr. N. Rupert Code G35, D. C. Peterson Dahlgren, VA 22448
10	Commander Naval Surface Weapons Center ATTN: Dr. S. Fishman (2 cys) Code R-13, F. J. Zerilli K. Kim E. T. Toton M. J. Frankel Code U-11, J. R. Renzi R. S. Gross Code K-22, F. Stecher J.M. Etheridge Silver Spring, MD 20910
3	Commander Naval Weapons Center ATTN: Code 31804, Mr. M. Smith Code 326, Mr. P. Cordle Code 3261, Mr. T. Zulkoski China Lake, CA 93555
6	Commander Naval Weapons Center ATTN: Code 3181, John Morrow Code 3261, Mr. C. Johnson Code 3171, Mr. B. Galloway Code 3831, Mr. M. Backman Mr. R.E. VanDevender, Jr. Dr. O. E. R. Heimdahl China Lake, CA 93555
3	Director Naval Research Laboratory ATTN: Dr. C. Sanday Dr. H. Pusey Dr. S. Zalesak Washington, DC 20375
2	Superintendent Naval Postgraduate School ATTN: Dir of Lib Dr. R. Ball Monterey, CA 93940
3	Long Beach Naval Shipyard ATTN: R. Kessler T. Eto R. Fernandez Long Beach, CA 90822
1	HQ USAF/SAMI Washington, DC 20330
1	AFIS/INOT Washigton, DC 20330
20	ADTC/DLJW (MAJ G. Spitale) Eglin AFB, FL 32542
10	ADTC/DLYV (Mr. J. Collins) Eglin AFB, FL 32542
1	AFATL/DLYV Eglin AFB, FL 32542
1	AFATL/DLODL Eglin AFB, FL 32542

DISTRIBUTION LIST

No. of Copies	Organization
1	AFATL/CC Eglin AFB, FL 32542
1	AFATL/DLODR Eglin AFB, FL 32542
1	HQ PACAF/DOOQ Hickam AFB Honolulu, HI 96853
1	HQ PACAF/OA Hickam AFB Honolulu, HI 96853
1	OOALC/MMWMC Hill AFB, UT 84406
1	HQ TAC/DRA Langley AFB, VA 23365
1	TAC/INAT Langley AFB, VA 23365
1	AUL-LSE 71-249 Maxwell AFB, AL 36112
1	AFWAL/MLLN (Mr. T. Nicholas) Wright-Patterson AFB, OH 45433
1	ASD/ENESS (S. Johns) Wright-Patterson AFB, OH 45433
1	ASD/ENFEA Wright-Patterson AFB, OH 45433
1	ASD/XRP Wright-Patterson AFB, OH 45433
1	HQUSAFE/DOQ APO New York 09012
1	COMIPAC/I-32 Box 38 Camp H. I. Smith, HI 96861
10	Battelle Northwest Laboratories PO Box 999 ATTN: G. D. Marr Richland, WA 99352
4	Director Lawrence Livermore Laboratory PO Box 808 ATTN: Dr. R. Werne Dr. J. O. Hallquist Dr. M. L. Wilkins Dr. G. Goudreau Livermore, CA 94550
6	Director Los Alamos Scientific Laboratory PO Box 1663 ATTN: Dr. R. Karpp Dr. J. Dienes Dr. J. Taylor Dr. E. Fugelso Dr. D. E. Upham Dr. R. Keyser Los Alamos, NM 87545
6	Sandia Laboratories ATTN: Dr. R. Woodfin Dr. M. Sears Dr. W. Herrmann Dr. L. Bertholf Dr. A. Chabai Dr. C. B. Selleck Albuquerque, NM 87115
1	Headquarters National Aeronautics and Space Administration Washington, DC 20546
1	Jet Propulsion Laboratory 4800 Oak Grove Drive ATTN: Dr. Ralph Chen Pasadena, CA 91102
1	Director National Aeronautics and Space Administration Langley Research Center Langley Station Hampton, VA 23365

DISTRIBUTION LIST

No. of Copies	Organization
1	US Geological Survey 2255 N. Gemini Drive ATTN: Dr. D. Roddy Flagstaff, AZ 86001
1	AAI Corporation PO Box 126 ATTN: R. L. Kachinski Cockeysville, MD 21030
1	Aerojet Ordnance Company 9236 East Hall Road Downey, CA 90241
1	Aeronautical Research Associates of Princeton, Inc. 50 Washington Road Princeton, NJ 08540
1	Aerospace Corporation 2350 E. El Segundo Blvd. ATTN: Mr. L. Rubin El Segundo, CA 90245
1	AVCO Systems Division 201 Lowell Street ATTN: Dr. Reinecke Wilmington, MA 01887
4	Boeing Aerospace Company ATTN: Mr. R. G. Blaisdell (M.S. 40-25) Dr. N. A. Armstrong C. J. Artura (M.S. 8C-23) Dr. B. J. Henderson (M.S. 43-12) P. O. Box 3999 Seattle, WA 98124
2	Brunswick Corporation 4300 Industrial Avenue ATTN: P. S. Chang R. Grover Lincoln, NE 68504
1	Computer Code Consultants, Inc. 1680 Camino Redondo ATTN: Dr. Wally Johnson Los Alamos, NM 87544
1	Dresser Center PO Box 1407 ATTN: Dr. M. S. Chawla Houston, TX 77001
1	Effects Technology, Inc. 5383 Hollister Avenue Santa Barbara, CA 93111
1	Electric Power Research Institute PO Box 10412 ATTN: Dr. George Sliter Palo Alto, CA 94303
2	Firestone Defense Research and Products 1200 Firestone Parkway ATTN: R. L. Woodall L. E. Vescelius Akron, OH 44317
1	FMC Corporation Ordnance Engineering Division San Jose, CA 95114
1	Ford Aerospace and Communications Corporation Ford Road, PO Box A ATTN: L. K. Goodwin Newport Beach, CA 92660
3	General Atomic Company PO Box 81608 ATTN: R. M. Sullivan F. H. Ho S. Kwei San Diego, CA 92138

DISTRIBUTION LIST

No. of Copies	Organization
1	General Dynamics PO Box 2507 ATTN: J. H. Caudros Pomona, CA 91766
1	General Electric Company Lakeside Avenue ATTN: D. A. Graham, Room 1311 Burlington, VT 05401
1	President General Research Corporation ATTN: Lib McLean, VA 22101
1	Goodyear Aerospace Corporation 1210 Massillon Road Akron, OH 44315
1	H. P. White Laboratory 3114 Scarboro Road Street, MD 21154
6	Honeywell, Inc. Government and Aerospace Products Division ATTN: Mr. J. Blackburn Dr. G. Johnson Mr. R. Simpson Mr. K. H. Doeringsfeld Dr. D. Vavrick Dr. C. Candland 600 Second Street, NE Hopkins, MN 55343
1	Hughes Aircraft Corporation ATTN: Mr. W. Keppel MS M-5, Bldg 808 Tucson, AZ 85706
2	Kaman Sciences Corporation 1500 Garden of the Gods Road ATTN: Dr. P. Snow Dr. D. Williams Colorado Springs, Co 80907
1	Lockheed Missile and Space Company 3251 Hanover Street ATTN: Org 5230, Bldg 201 Mr. R. Robertson Palo Alto, CA 94304
1	Lockheed Missiles and Space Company PO Box 504 ATTN: R. L. Williams Dept. 81-11, Bldg 154 Sunnyvale, CA 94086
1	Materials Research Laboratory Inc. 1 Science Road Glenwood, IL 60427
2	McDonnell-Douglas Astronautics Company 5301 Bolsa Avenue ATTN: Dr. L. B. Greszcuk Dr. J. Wall Huntington Beach, CA 92647
1	New Mexico Institute of Mining and Technology ATTN: TERA Group Socorro, NM 87801
1	Northrop Corporation 3901 W. Broadway ATTN: R. L. Ramkumar Hawthorne, CA 90250
1	Nuclear Assurance Corporation 24 Executive Park West ATTN: T. C. Thompson Atlanta, GA 30245
2	Orlando Technology, Inc. PO Box 855 ATTN: Mr. J. Osborn Mr. D. Matuska Shalimar, FL 32579

DISTRIBUTION LIST

No. of Copies	Organization
1	Rockwell International Missile Systems Division ATTN: A. R. Glaser 4300 E. Fifth Avenue Columbus, OH 43216
3	Schumberger Well Services Perforating Center ATTN: J. E. Brooks J. Brookman Dr. C. Aseltine PO Box A Rosharon, TX 77543
1	Science Applications, Inc. 101 Continental Building Suite 310 El Segundo, CA 90245
1	Systems, Science and Software PO Box 1620 ATTN: Dr. R. Sedgwick La Jolla, CA 92037
2	TRW Systems Group One Space Park, R1/2120 ATTN: D. Ausherman M. Bronstein Redondo Beach, CA 90278
1	United Technologies Research Center 438 Weir Street ATTN: P. R. Fitzpatrick Glastonbury, CT 06033
1	US Steel Corporation Research Center 125 Jamison Lane Monroeville, PA 15146
1	VPI & SU 106C Norris Hall ATTN: Dr. M. P. Kamat Blacksburg, VA 24061
2	Vought Corporation PO Box 225907 ATTN: Dr. G. Hough Dr. Paul M. Kenner Dallas, TX 75265
1	Westinghouse, Inc. PO Box 79 ATTN: J. Y. Fan W. Mifflin, PA 15122
1	Drexel Institute of Technology Department of Mechanical Engr. ATTN: Dr. P. C. Chou 32d and Chestnut Streets Philadelphia, PA 19104
3	Southwest Research Institute Dept of Mechanical Sciences ATTN: Dr. U. Lindholm 8500 Culebra Road San Antonio, TX 78228
1	Southwest Research Institute ATTN: Dr. C. Anderson 6220 Culebra Road San Antonio, TX 78284
4	SRI International 333 Ravenswood Avenue ATTN: Dr. L. Seaman Dr. L. Curran Dr. D. Shockey Dr. A. L. Florence Menlo Park, CA 94025

DISTRIBUTION LIST

No. of Copies	Organization
2	University of Arizona Civil Engineering Department ATTN: Dr. D. A. DaDeppo Dr. R. Richard Tucson, AZ 85721
1	University of Arizona School of Engineering ATTN: Dean R. Gallagher Tucson, AZ 85721
1	University of California ATTN: Dr. M. Ziv 504 Hilgard Avenue Los Angeles, CA 90024
1	University of California Department of Physics ATTN: Dr. Harold Lewis Santa Barbara, CA 93106
2	University of California College of Engineering ATTN: Prof. W. Goldsmith Dr. A. G. Evans Berkeley, CA 94720
2	University of Delaware Department of Mechanical Engineering ATTN: Prof. J. Vinson Dr. M. Taya Newark, DE 19711
1	University of Denver Denver Research Institute ATTN: Mr. R. F. Recht 2390 S. University Blvd. Denver, CO 80210
2	University of Florida Department of Engineering Sciences ATTN: Dr. R. L. Sierakowski Dr. L. E. Malvern Gainesville, FL 32601
1	University of Oklahoma School of Aerospace, Mechanical and Nuclear Engineering ATTN: Dr. C. W. Bert Norman, OK 73069
1	West Virginia University Department of Mechanical and Aerospace Engineering ATTN: Dr. N. J. Salamon Morgantown, WV 26506
1	University of Daytona Impact Physics Research Institute ATTN: Dr. S. J. Bless 300 College Park Daytona, OH 45406

Aberdeen Proving Ground

Dir, USAMSAA
ATTN: DRXSY-D
DRXSY-MP, H. Cohen
Cdr, USATECOM
ATTN: DRSTE-TO-F
Dir, USAMTD
ATTN: Mr. W. Pless
Mr. S. Keithley

Cdr, CRDC, AMCCOM
ATTN: DRSMC-CLB-PA
DRSMC-CLN
DRSMC-CLJ-L

USER EVALUATION OF REPORT

Please take a few minutes to answer the questions below; tear out this sheet, fold as indicated, staple or tape closed, and place in the mail. Your comments will provide us with information for improving future reports.

1. BRL Report Number _____

2. Does this report satisfy a need? (Comment on purpose, related project, or other area of interest for which report will be used.)

_____

_____

_____

3. How, specifically, is the report being used? (Information source, design data or procedure, management procedure, source of ideas, etc.) _____

_____

_____

4. Has the information in this report led to any quantitative savings as far as man-hours/contract dollars saved, operating costs avoided, efficiencies achieved, etc.? If so, please elaborate.

_____

_____

5. General Comments (Indicate what you think should be changed to make this report and future reports of this type more responsive to your needs, more usable, improve readability, etc.) _____

_____

_____

_____

6. If you would like to be contacted by the personnel who prepared this report to raise specific questions or discuss the topic, please fill in the following information.

Name: _____

Telephone Number: _____

Organization Address: _____

_____

_____